Acta Crystallographica Section D
Biological Crystallography
ISSN 0907-4449

Three-dimensional structure of an immunoglobulin light-chain dimer with amyloidogenic properties

Philip C. Bourne,[a] Paul A. Ramsland,[a]† Lin Shan,[a] Zhao-C. Fan,[a] Christina R. DeWitt,[a] Brandon B. Shultz,[a] Simon S. Terzyan,[a] Carolyn R. Moomaw,[b] Clive A. Slaughter,[b] Luke W. Guddat[a]‡ and Allen B. Edmundson[a]*

[a]OMRF, 825 N E 13th Street, Oklahoma City, Oklahoma 73104, USA, and [b]University of Texas Southwestern Medical School, Howard Hughes Medical Institute, 5323 Harry Hines Boulevard, Dallas, Texas 75235, USA

† Present address: Structural Biology Laboratory, The Austin Research Institute, Studley Road, Heidelberg, Vic 3084, Australia.
‡ Present address: Department of Biochemistry, The University of Queensland, St Lucia, Qld 4072, Australia.

Correspondence e-mail: allen-edmundson@omrf.ouhsc.edu

Received 8 October 2001
Accepted 4 March 2002

PDB Reference: immunoglobulin light-chain dimer, 1jvk, r1jvksf.

The X-ray structure of an immunoglobulin light-chain dimer isolated from the urine as a 'Bence-Jones protein' from a patient with multiple myeloma and amyloidosis (Sea) was determined at 1.94 Å resolution and refined to R and $R_{\rm free}$ factors of 0.22 and 0.25, respectively. This 'amyloidogenic' protein crystallized in the orthorhombic $P2_12_12_1$ space group with unit-cell parameters a = 48.28, b = 83.32, c = 112.59 Å as determined at 100 K. In the vital organs (heart and kidneys), the equivalent of the urinary protein produced fibrillar amyloid deposits which were fatal to the patient. Compared with the amyloidogenic Mcg light-chain dimer, the Sea protein was highly soluble in aqueous solutions and only crystallized at concentrations approaching 100 mg ml^{-1}. Both the Sea and Mcg proteins packed into crystals in highly ordered arrangements typical of strongly diffracting crystals of immunoglobulin fragments. Overall similarities and significant differences in the three-dimensional structures and crystalline properties are discussed for the Sea and Mcg Bence-Jones proteins, which together provide a generalized model of abnormalities present in λ chains, facilitating a better understanding of amyloidosis of light-chain origin (AL).

1. Introduction

Amyloidosis of immunoglobulin light-chain origin (AL) belongs to a group of diseases known as plasma-cell dyscrasias (Falk *et al.*, 1997; Stone, 1990). AL can be found in the presence or absence of multiple myeloma, which is characterized by multiple tumors of the bone marrow. Fibrils of amyloid are composed of intact or fragmented monoclonal light chains synthesized by plasma cells, which are commonly found in increased numbers in the bone marrow of patients with AL or multiple myeloma (Buxbaum *et al.*, 1990). While treatment for AL has been unsatisfactory in the past, attempts have been made to use alkylating agents or other medicinals known to be effective in reducing plasma-cell proliferation like that found in multiple myeloma (Kyle *et al.*, 1997; Pascali, 1995). New approaches being developed for the treatment of AL include the use of humanized antibodies directed against the causative light chains (Alan Solomon, personal communication).

In approximately 10% of subjects with multiple myeloma, the light chains (L-chains) exit the blood stream and precipitate as pathological amyloid deposits in vital organs such as the kidney, heart, tongue and skin (Glenner, 1980; Glenner *et al.*, 1971; Kyle & Gertz, 1995; Osserman *et al.*, 1964; Solomon & Weiss, 1995). Clinical diagnosis typically begins with nephropathy accompanied by Bence-Jones proteinuria. While the latter can be asymptomatic in the early stages, the disease

progresses through a nephrotic syndrome to renal failure. Preferential deposition of AL fibrils in the heart myocardium tends to be dominant, but often remains unconfirmed until autopsy. For more definitive diagnoses, clinical findings may be supplemented by histochemical, electrophoretic, antigenic and amino-acid sequence analyses of the amyloid-infiltrated tissues. One of the most common staining procedures utilizes Congo red to produce a green birefringence under polarizing light. Alternatively, electron microscopy may be employed to scan the tissues for diagnostic amyloid fibrils. Morphologically, fibrillar deposits of AL are indistinguishable from amyloid fibrils produced by other precursors in at least 18 diseases (Wall *et al.*, 1999), including diabetes and Alzheimer's disease. These deposits are characterized by unbranched fibrils 80–110 Å in diameter (Glenner *et al.*, 1971). Fiber-diffraction methods demonstrated that the principal underlying structures of AL fibrils were β-pleated sheets, in which the directions of the β-strands were perpendicular to the long axes of the fibrils (Glenner, 1980; Sunde & Blake, 1997).

For the studies described in the present article, Bruce D. Cheson MD, an oncologist at the University of Utah Medical Center, identified a patient (Sea) with multiple myeloma and amyloidosis associated with a λ-type immunoglobulin L-chain. We confirmed his diagnosis by showing that the Sea Bence-Jones dimer, together with two other amyloidogenic λ-chains (Mcg and Bla) and one κ chain (Jen), formed amyloid fibrillar deposits in fibroblast monolayer cell cultures (Harris *et al.*, 2000). These deposits gave a green birefringence when stained with Congo red. After 48 h, fine filaments were found to be interspersed with nascent collagen (types I and III) synthesized by the fibroblasts. By 72 h, the fine filaments had developed into dense amyloid fibrils.

Amyloid fibrillogenesis was observed to impede the maturation of collagen, as evidenced by the absence of characteristic black-and-white banding patterns in electron micrographs. Using fluroescein- and gold-labelled anti-L-chain antibodies, the amyloidogenic L-chains were observed to decorate the surfaces of the nascent collagen strands. After 72 h, amyloid fibrils were wedged into bundles of nascent collagen, causing the latter to disintegrate. As a control, we selected a λ-type Bence-Jones protein from a myeloma patient (Hud) who showed no symptoms or signs of AL amyloidosis. In electron micrographs of fibroblast monolayers bathed with the Hud protein, we were not able to detect amyloid fibrils. Collagen produced by the fibroblasts passed smoothly through nascent stages to the fully developed cross-linked fibers with alternating black-and-white banding patterns.

These results strongly suggested that the amyloidogenic L-chains were attracted to and trapped in perivascular tissues by antigen–antibody-like reactions. Such an assumption was supported by previous crystallographic studies of complexes of the prototypic amyloidogenic dimer from Mcg with more than 80 small organic molecules and peptides (Edmundson *et al.*, 1975, 1984, 1987, 1993; Edmundson & Ely, 1985; Herron *et al.*, 1985). Each of these ligands was bound in the designated active site and in no other location. After our demonstration that the Mcg dimer showed binding activity for dinitrophenyl compounds, Osserman's group found that similar haptens bound to seven other Bence-Jones proteins from subjects with documented amyloidosis but not to six L-chains derived from myeloma patients without AL (Bertram *et al.*, 1980).

In other studies related to the present work, we tried to develop model systems covering both the Sea and Mcg proteins. However, preliminary results with the Mcg dimer were too destructive to be extended to Sea. When collagen-like synthetic polymers such as $(\text{Gly-Pro-Pro})_5$ and $(\text{Gly-hydroxy-Pro-Pro})_s$ were diffused into pre-existing Mcg crystals, widespread structural alterations were detected in both the VL and CL domains by difference Fourier analysis. On a positive note, these structural alterations could be completely prevented by pre-treatment of the crystals with blocking agents specific for the Mcg active site (*e.g.* the collagenase substrate PZ-Pro-Leu-Gly-Pro-D-Arg, where PZ is a 4-phenylazobenzyloxycarbonyl moiety; Wünsch & Heidrich, 1963).

2. Experimental

2.1. Purification and crystallization of the Sea Bence-Jones dimer

The Sea Bence-Jones protein was isolated and purified by methods described previously (Alvarado *et al.*, 2001). Final steps in purification were based on gel filtration over Sephacyl S-200 and ion-exchange chromatography on DEAE-cellulose. The DEAE step was essential to remove a yellow urinary pigment from the samples of Bence-Jones protein isolated by precipitation from the urine with 2 *M* ammonium sulfate. Unusually in relation to other light chains, Fv and Fab samples in our collection, the Sea dimer was inordinately soluble in aqueous and PEG solutions. Therefore, extreme conditions were necessary for producing large crystals suitable for X-ray analysis with conventional in-house equipment. Several methods of crystallization were used with different degrees of success, all with polyethylene glycol (PEG 8000) at temperatures ranging from 277 to 295 K. Finally, a new method was introduced to promote crystallization of the Sea dimer (Alvarado *et al.*, 2001). To stimulate nucleation, a sample dissolved in PEG 8000 in a glass capillary was subjected to rapid dehydration through vapor diffusion of water across an air gap into a strong absorbent (100% glycerol) for a relatively short duration (12 h). The absorbent was then weakened to 80% glycerol for slower growth of the crystals over a longer period (at least 13 d). Initial protein concentrations were required to be greater than twice those required for crystallization of other more typical L-chains. Dehydration techniques drove the effective concentrations toward values of 100 mg ml^{-1}.

Crystals prepared by these methods belong to space group $P2_12_12_1$, with unit-cell parameters a = 48.99, b = 85.15, c = 113.89 Å, $\alpha = \beta = \gamma = 90^\circ$ (as determined at ambient temperature). The crystals diffracted to high resolution but were sensitive to radiation damage from the X-ray beam. Unless they were more than 0.3 mm in thickness, they

dissolved in about 20 h at ambient temperatures in an X-ray beam generated by a rotating anode operating at 50 kV and 90 mA. However, larger crystals decayed slowly enough to yield diffraction data that were 98% complete in 36 h. These problems were circumvented by flash-freezing of the crystals and collection of X-ray diffraction data at 100 K.

2.2. Collection of X-ray diffraction data

X-ray diffraction data were collected at ambient temperatures at the Photon Factory, Tsukuba, Japan. Although sufficient to determine an initial structure for the Sea dimer, radiation damage to the crystal resulted in an incomplete data set (46% overall). It was therefore necessary to collect data of higher quality. Diffraction data were collected at 100 K using a Rigaku RUH3R rotating-anode generator with an R-AXIS IV image-plate detector. For these studies, the crystals were transferred to a cryoprotectant solution of 8% PEG 8000 and 28% PEG 400. At 100 K, the unit cell was found to have contracted to a = 48.28, b = 83.32, c = 112.59 Å. All data collected on the R-AXIS IV image plate were reduced and scaled using the programs *DENZO* and *SCALEPACK* (Otwinowski & Minor, 1997). Statistics for these data are presented in Table 1.

2.3. Determination of the amino-acid sequence of the Sea λ-chain

As in many λ-chains (Kabat *et al.*, 1991), the N-terminal residue was cyclized to pyrrolidone carboxylic acid (PCA or pyroglutamate). After removal of the blocked end group with pyroglutamyl aminopeptidase, the first 40 residues were identified by repetitive Edman degradation with an automated sequencer. Ambiguities in the sequence of the last part of this segment were resolved by detailed examinations of soluble peptides obtained by proteolytic digestion with trypsin. Other peptides in the tryptic series covered the remainder of the VL (variable domain of the L-chain). In checking the sequence against electron-density maps of the Sea dimer, we found no discrepancies between the chemical and crystallographic residue assignments.

2.4. Determination of the three-dimensional structure of the Sea dimer

The crystal structure was solved by the molecular-replacement method (Fitzgerald, 1988; Rossmann, 1990), using the preliminary synchrotron X-ray diffraction data. Rotation-function calculations (Crowther, 1972; Crowther & Blow, 1967) were initially performed with the *MERLOT* program package (Fitzgerald, 1988), with X-ray diffraction data in the resolution range 15–4.0 Å. The complete Mcg dimer was used as a starting model, but since this procedure did not produce a clear-cut solution, the starting model was changed to a heterologous L-chain dimer engineered from Mcg and Hud monomers (Allen Edmundson *et al.*, unpublished work). Disulfide-linked heterologous dimers can be produced if one monomer (*e.g.* Mcg—S—) is reduced and the second is converted to a mixed disulfide (*e.g.* Hud—S—S—pyridine). This treatment (Peabody *et al.*, 1980; Shaw *et al.*,

Table 1
Summary of data collection at 100 K and statistics for the model refinement.

Values in parentheses are for the outer resolution shell.

	Sea model
Resolution range (Å)	30.0–1.94 (2.01–1.94)
Completeness	98.2 (89.1)
$R_{\rm sym}$†	0.043 (0.319)
$\langle I\rangle/\langle\sigma(I)\rangle$	29.6 (3.78)
Redundancy	4
Unique reflections	33848
Final $R_{\rm cryst}$‡ (%)	22.3
$R_{\rm free}$ (5% total data) (%)	25.4
No. of protein residues	429
Average B factor (protein) (Å^2)	34.65
No. of water molecules	264
Average B factor (solvent) (Å^2)	39.18
R.m.s. deviations from ideality	
Bond lengths (Å)	0.01
Bond angle (°)	1.73
R.m.s. deviations from ideality in B factors (Å^2) (values in parentheses are for the target)	
Main-chain bonds	1.684 (1.5)
Main-chain angles	2.739 (2.0)
Side-chain bonds	2.317 (2.0)
Side-chain angles	3.299 (2.5)

† $R_{\rm sym} = \sum_h \sum_J |\langle I_h\rangle - I_J(h)|/\sum_h \sum_J I(h)$, where $I(h)$ is the intensity of reflection h. $\sum_h$ is the sum over all reflections and $\sum_J$ is the sum over J measurements of the reflection. ‡ $R_{\rm cryst} = \sum \big||F_o| - |F_c|\big|/\sum |F_o|$.

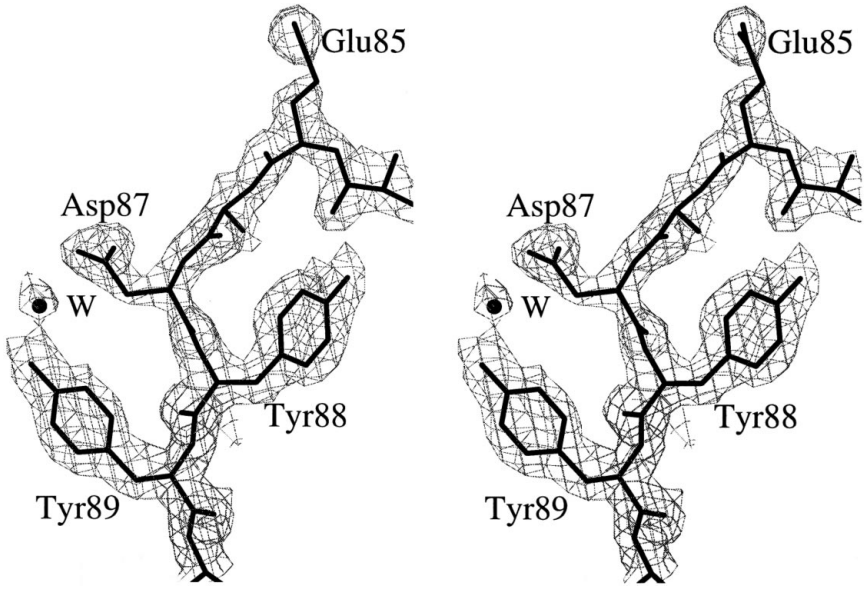

Figure 1
An example of electron density from the final $2F_o - F_c$ map contoured at $2\sigma(\rho)$. The figure was generated with the program *BOBSCRIPT* (Esnouf, 1997). The selected segment belongs to FR3 and immediately precedes the second inter-chain Cys residue and CDR3 of monomer *B*.

```
                              |     CDR1     |
              10        20     27abc        35
SEA     XTALTQPAS- VSGSPGQSIT VSCTGVSSIVGSY NLVSW
MCG     .S.....P.- A...L...V. I....T..D..G. .Y...

                         |  CDR2  |
        40         50         60         70
SEA     YQQHP GKAPKLLTYE VNKRPSGVSD RFSGSKSGNS ASLTI
MCG     ....A .....VII.. ........P. .........T ....V

                        |  CDR3      |
        80         90     95ab  100       109
SEA     SGLQA EDEADYYCSS YDGSSTSVVFGG GTKLTVLGQ
MCG     ..... .......... .E..DN-F...T ...V.....
```

Figure 2
Amino-acid sequences of the VL domains of the Sea and Mcg λ-type Bence-Jones dimers. The three hypervariable loops are labeled CDR1, CDR2 and CDR3. One-letter codes for the amino-acid residues are numbered according to the system of Kabat *et al.* (1991). A gap is left at position 10, which corresponds to a deletion in the λ-chain sequences. Insertions in the Sea and Mcg sequences but not in all light chains are designated 27a, 27b, 27c and 95a. An extra serine residue is found in position 95b of Sea, but is absent in the Mcg sequence. Note that there are only eight differences in the 32 positions of the three CDRs. The two molecules belong to the same VL subgroup (λII) and both act as precursors in lethal amyloid fibrillogenesis. In other figures, please note that the PDB format is followed for numbering residues without gaps or insertions in the sequence. Figs. 1, 6 and 7 in particular deviate slightly from the Kabat numbering system.

1987) ameliorates the overwhelming preference for self-dimerization, rather than similar interactions with heterologous light chains (Stevenson & Straus, 1968). The three-dimensional structure of the Mcg × Hud hybrid has been determined to 1.8 Å resolution and is being prepared for publication.

The elbow bend angle of this hybrid dimer was increased stepwise from the initial value of 113° by 40° in 10° intervals and each modified structure was examined by the molecular-replacement method. An elbow bend is defined as the angle subtended by the pseudodyad between the VL1 and VL2 domains and the pseudo-twofold axis between CL1 and CL2. A single peak was obtained when the elbow bend angle was expanded by 20°. Results obtained with other modifications of the starting probe were less convincing. When the diffraction data collected at 100 K became available, the preliminary model was refined against these data using the *CNS* suite of programs (Brünger *et al.*, 1998) and *REFMAC*5 (Murshudov *et al.*, 1999). The same set of reflections was used to calculate $R_{\rm free}$ (Brünger, 1992) for refinement with *CNS* and *REFMAC*5. The current *R* factor is 0.22 for all data in the resolution range 30–1.94 Å. From 5% of randomly distributed reflections, $R_{\rm free}$ was calculated to be 0.25 (see Table 1). In the Ramachandran plot, as defined with the program *PROCHECK* (Laskowski *et al.*, 1993), 88.2% of the non-glycine residues were located in the most favored regions. An example of the final $2F_o - F_c$ electron density is presented in Fig. 1. Final model coordinates have been deposited in the PDB (Berman *et al.*, 2000).

3. Results and discussion

3.1. Amino-acid sequence of the Sea protein

The amino-acid sequence of the Sea λ-chain is presented in Fig. 2, which also includes the Mcg sequence for comparison. The Mcg immunoglobulin was originally classified as subgroup V of λ-chains (Kabat & Wu, 1991). After extensive additions to the sequence database, both Mcg and Sea proteins are now considered to belong to subgroup II (Alan Solomon, personal communication). Each Sea monomer was longer than the Mcg λ-chain by one amino-acid residue. This difference was localized to the CDR3 segment, which contains an extra serine residue in Sea [a product of the joining (J) gene]. Overall, there were 23 substitutions in the Sea VL sequence relative to that in the Mcg protein.

3.2. Solubility differences between the Sea and Mcg dimers

The Sea dimer is considerably more soluble than the Mcg protein in aqueous solutions. For example, the Mcg dimer has euglobulin properties and the Sea dimer does not. It seems likely that these differences are attributable to the VL domains, since the C domains have only four sequence interchanges. In the Sea dimer there are 12 more VL serines located in surface positions accessible to solvent. Overall counts of polar and hydrophobic side chains are otherwise quite similar in the two dimers. *GRASP* plots (Nicholls *et al.*, 1991) and hydrophilicity plots do not reveal features clearly related to the disparities in solubility.

However, solubility differences were manifested in the crystallization trials for the two proteins. For instance, crystallization of the Sea dimer was difficult to achieve until the final protein concentration approached 90–100 mg ml^{-1} immediately before nucleation and crystal growth. When urinary samples containing 4 mg ml^{-1} of Mcg Bence-Jones protein were dialyzed against deionized water for 12 h at 277 K, approximately 50% of the protein crystallized as long thin plates and the other half remained in solution. With highly purified samples of the Mcg dimer, diffraction-quality crystals could be produced in capillaries by slow dialysis against deionized water at ambient temperature (Abola *et al.*, 1980; Ely *et al.*, 1989).

3.3. Comparison of the general features of the Sea and Mcg dimers

As mentioned earlier, the Sea dimer crystallized in PEG 8000 in the orthorhombic space group $P2_12_12_1$, with the asymmetric unit consisting of a dimer with a total of 434 amino-acid residues. In ammonium sulfate the Mcg dimer formed crystals with the trigonal space group $P3_121$ and unit-cell parameters $a = b = 72.3$, $c = 185.9$ Å, $\alpha = \beta = 90$, $\gamma = 120°$; the asymmetric unit was a dimer with 432 residues. Unit-cell volumes were 475 092 Å^3 for the Sea crystals (analysed at ambient temperature) and 838 420 Å^3 for the Mcg crystals. There were four asymmetric units in the Sea unit cell and six in the Mcg cell. By Matthews' procedure (Matthews, 1968), the

partial solvent volumes (V_{solv}) in the Sea and Mcg unit cells were estimated to be 47.8 and 56.0%, respectively.

We have emphasized that the Sea dimer differs in shape, solubility and physical characteristics from the Mcg protein. Rotation angles relating VL1 and VL2, and CL1 and CL2 were calculated to be very close to exact dyads (179.6°) in the Sea protein. Measurements of the elbow bend angles between the pseudodyads of the VL and CL pairs of domains were based on comparisons of residues (38 from VL and 34 from CL) from the most ordered portions of the β-pleated sheets (Edmundson *et al.*, 1975). The elbow bend angles were 133.6° in the Sea dimer and 113.0° in the Mcg dimer. This difference helps to explain why the determination of the Sea structure was facilitated by an increase of 20° in the elbow bend of the Mcg × Hud heterologous dimer used as the starting model.

Dissecting the models more thoroughly, we found that both L- and H-chain analogs in the Sea protein were more extended than in the Mcg molecule. For instance, the angles between VL and CL in the L-chain analogs were 118.1° in Sea and 110.5° in Mcg, while the corresponding angles in the H-chain analogs were 70.8° (Sea) and 43.5° (Mcg). Such large differences in the segmental flexibility of domains were reflected in the crossing angles between the VL1 and VL2 and the CL1 and CL2 domains in the Fab-like dimers. For example, the VL1 and VL2 domains crossed each other at an angle of 73.8° in the Sea dimer and 96.4° in the Mcg dimer. Relationships between CL1 and CL2 were more similar in the two proteins: the crossover angles were 88.3° in Sea and 91.0° in Mcg.

3.4. Comparison of CDR1 and CDR3 in the Sea and Mcg dimers

Ribbon models for the Sea and Mcg dimers are shown in Fig. 3. Examinations of these three-dimensional structures reveal differences that are also important in determining the solubility of each molecule. Despite having the same number of residues as Mcg, the CDR1 loops of the Sea dimer protrude into bulk solvent to a significantly greater extent (see Fig. 4). Moreover, the Sea dimer is more extended than the Mcg protein, as evidenced by the observation that the elbow bend angle in the Sea dimer is 20° greater. Practical consequences are greater exposures of segments in the interface between the V and C domains and particularly more accessibility of the surface residues of the CL domain of monomer *B*.

While not directly expanding the crown of the CDR3 loop, the insertion of the extra serine residue in Sea affected not only the size but also the shape of this hypervariable region. Relative to the Mcg dimer, the CDR3 loops in the two conformational isomers of the Sea protein were much more convoluted, especially at the top (see Fig. 5). Conformational differences between the CDR3s in the two Sea monomers are also worthy of comment. Although the electron density for the LCDR3 of monomer *A* was relatively weak, it was sufficient to discern these obvious differences in main-chain conformations. In the light-chain analog (Sea monomer *A*), the CDR3 loop was contorted at its crest. Its vertical position was lower than that of the adjacent CDR1. In contrast, CDR3 in the heavy-chain analog (monomer *B*) was longer and thinner and was situated in a position above that of CDR1. At the base, the two CDR3s were superimposable for the first three residues of the ascending segment and the last three residues of the descending arm.

CDR1 of monomer *A* cannot maintain the same conformation as in monomer *B* owing to steric restraints imposed by the packing of the molecules in the crystal lattice. Residues Ser13*A* and Pro14*A* in a symmetry-related molecule occupy the position that would otherwise be allocated to Ser27*A*. Superposition of the framework regions of monomers *A* and *B* show that chain *A* is distorted from residues 25*A* to 34*A*. The repositioning of CDR1 has the knock-on effect of distorting CDR3. Tyr93*A*, usually an important ligand-contact residue, is pushed aside by Ile28*A*. These concerted changes in the orientations of CDRs 1 and 3 in monomer *A* probably explain the results of attempts to co-crystallize the Sea dimer with the methyl ester of Asp-Phe (aspartame), which binds to the

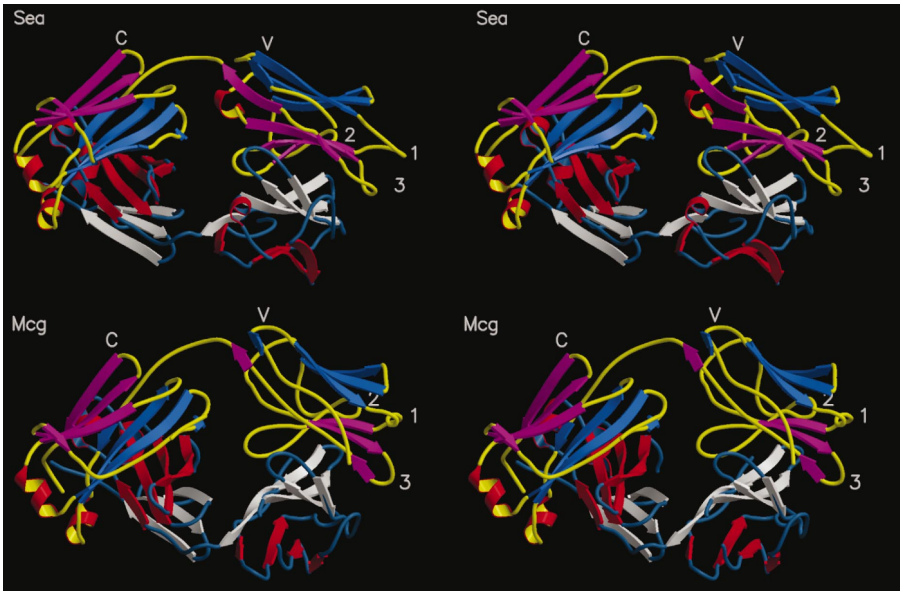

Figure 3
Comparison of the Sea and Mcg Bence-Jones dimers. The models and stereo diagrams were constructed with the program *MOLSCRIPT* (Kraulis, 1991). Each dimer mimics an Fab in appearance. Yellow tubular segments represent the isomer more nearly approximating the conformation of the light-chain component of an Fab; steel blue tubes correspond to the heavy-chain analogs. Pairs of variable domains (V) are on the right and constant domain pairs (C) are on the left. Strands of β-pleated sheets are shown as directional arrows, with the four-stranded layers colored blue and red in the L- and H-chain conformational isomers. Helices (some distorted) are depicted as red and yellow spirals. CDRs are numbered 1, 2 and 3. Note that the Sea dimer is more extended than the Mcg dimer (elbow bend angle of 133° *versus* 113° for Mcg) and the β-pleated sheets are more regular.

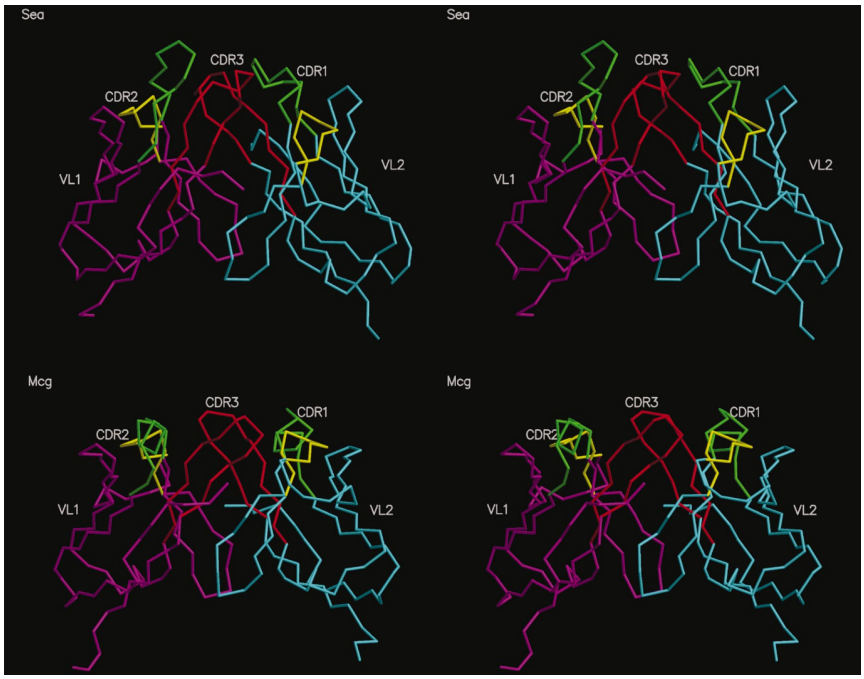

Figure 4
Stereo diagrams showing the comparison of the V domain pairs from the Sea and Mcg Bence-Jones dimers. 'Framework' regions (FRs) are shown in magenta for the L-type isomers (monomer *A*) and are labeled VL. H-chain analogs (monomer *B*) have cyan-colored FRs and are marked VH. All CDR1 loops are colored green, CDR2s yellow and CDR3s red. Note the differences in spatial relationships of CDR1 and CDR3 loops in the Sea dimer with respect to those in Mcg. The Sea pair is more upright and the CDR1 loops protrude farther out into the bulk solvent. This figure was generated with the program *MOLSCRIPT* (Kraulis, 1991).

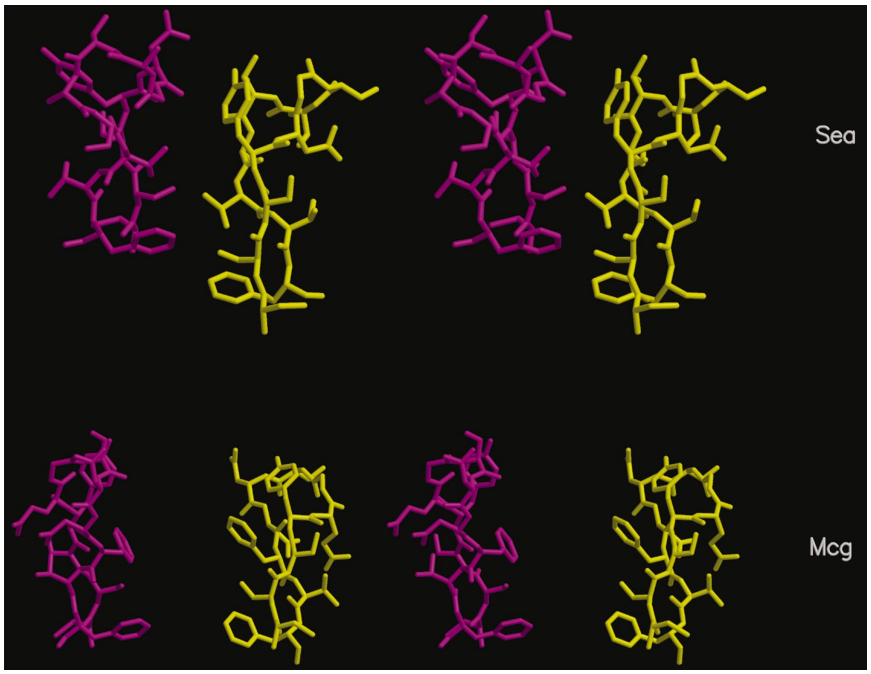

Figure 5
Comparison of the CDR3s of the Sea and Mcg Bence-Jones dimers, presented as stereo diagrams. Components of monomer *B* (H-chain analogs) are colored magenta and segments of monomer *A* (L chains) are yellow. CDR3 loops act as pillars of the active sites and their relative locations in each dimer largely determine the magnitudes of the openings into the binding cavities. This opening is significantly narrower in the Sea dimer (8 *versus* 15 Å), but the depths are practically the same. The phenylalanine residues at the lower ends mark the floors of the cavities. This figure was prepared with the program *MOLSCRIPT* (Kraulis, 1991).

protein with moderately high affinity (K_d = 10^{-7} *M*) in solution (C. R. DeWitt and A. B. Edmundson, unpublished data). Under conditions in which the ligand:protein molar ratio was kept at 10:1 in the PEG 8000 crystallizing medium, the crystals which emerged were identical in appearance to those in the unliganded protein. Difference Fourier analysis of this crystal form indicated that the peptide ligand was not present in the active site in the Sea dimer. We concluded that the conformational distortions of CDRs 1*A* and 3*A* required for crystallogenesis in this particular habit were only possible in Sea protein molecules devoid of bound ligand.

Interactions between CDR3 and CDR1 were different in the two monomers, as expected from their dissimilar shapes and relative orientations. In monomer *B*, the ladder of hydrogen bonds between the descending arm of CDR1 and the ascending arm of CDR3 retained the classical relationship of two adjacent antiparallel β-strands in a pleated sheet. Both of these β-strands were members of a five-stranded β-pleated sheet. As a guide to the alignment, dual hydrogen bonds were formed between the NH and CO groups of the polypeptide backbone at Ser36 of CDR1 with the CO and NH groups of Ser91 of CDR3. The third hydrogen bond was made between the CO of Leu34 and the NH of Tyr93. Near the crests of the two loops, a hydrogen bond was formed between the CO of Val29 and the NH of Gly95 only in monomer *B*. This hydrogen bond was the key to the close positioning of the two loops. Because of the relative differences in size and shape of the two CDRs in monomer *A*, the ladder of inter-strand hydrogen bonds was limited to the first two residues of CDR1. These differences are clearly evident in Fig. 6.

3.5. Packing interactions of the Sea dimer

Prominent packing interactions involve the first three residues of the monomer *A* VL domain. Interactions of monomer *A* fall under the precepts of our triad hypothesis (Edmundson *et al.*, 1998, 1999) for the formation of extended β-pleated sheets by pairing of antiparallel β-strands from symmetry-related dimers across twofold axes in the crystal lattice. Unlike other examples of such packing, the outermost

segment (designated 4-1) of the reference VL domain is paired with the second β-strand (numbered 4-2) of an antiparallel pleated sheet in a symmetry-related molecule. The carbonyl O atom of the pyrrolidone carboxylic acid (PCA) in position 1 of the reference molecule is hydrogen bonded to the NH group of Thr19 in β-strand 4-2 of monomer *A* in an adjacent Sea dimer. The NH and terminal O atom of PCA 1 also form hydrogen bonds with the CO of Thr19. Hydrogen bonds 4 and 5 are formed by interactions of the NH and CO groups of Ala3 with the CO and NH groups of Ser17. In the other direction, Ser17 and Thr19 of the reference molecule hydrogen bond with PCA1 and Ala3 of a third dimer. The binding pattern is repeated throughout the crystal to produce ribbons of Sea dimers of indefinite length (see Fig. 7).

This type of packing arrangement was only possible using monomer *A*, as VL segments 4-1 and 4-2 in monomer *B* are not in the appropriate orientations after formation of the *AB* VL dimer. In the original formulation of the triad hypothesis, at least four hydrogen bonds were expected to be contributed by three pairs of residues. Therefore, while elegant, the stacking pattern of backbone atoms alone falls short of the stabilization required in the Sea crystal lattice. Two additional hydrogen bonds (6 and 7) involving side chains compensate for these deficiencies. A sixth interaction occurs between the hydroxyl group of Thr2 in the reference molecule and the main-chain amide group of Gly15 in the second dimer. Finally, a seventh hydrogen bond links the hydroxyl groups of Thr5 and Ser17.

3.6. Description of the β-pleated sheets

In the Sea monomers the β-pleated sheets are generally more ordered with respect to their hydrogen-bonding patterns than they are in the Mcg dimer. This finding partly arises from the lack of crowding at the junction of the VL and CL domains in monomer *B* of the Sea dimer. In Mcg, the acute bend between these domains tends to disrupt regular structures on both sides of the bend (see next paragraph). Sea VL domains in monomer *A* and monomer *B* have an obvious four-stranded layer that is actually partitioned into three strands of antiparallel β-pleated sheet and a fourth outer β-strand. The latter is stabilized mainly by parallel hydrogen bonding with the most lateral β-strand of the second pleated sheet in the sandwich structure of the VL domain. As in Mcg, this second β-pleated sheet does not strictly conform to five antiparallel strands, because the two pillars supporting the CDR2 loop are not sufficiently ordered to classify them as complete β-strands. However, the ascending pillar for CDR2 does have a short segment of β-structure, which interlocks with the other β-strands at the outer edge of the sheet. The connecting segment between CDR3 with the CL domain has two segments of β-structure separated by a 'β-bulge' corresponding to a Phe-Gly-Gly-Gly sequence in the first part of VL framework 4 (see residues 98–101 in Fig. 2). These arrangements of β-strands within the VL and CL domains of monomers *A* and *B* are shown as stereo diagrams in Fig. 3 for both the Sea and Mcg dimers.

In the Sea C domains of both monomers *A* and *B*, the four-stranded β-pleated sheets are again more regular than in the Mcg dimer. The irregularity in Mcg monomer *B* is propagated in the forward direction to VL and distally into CL by spatial congestion of chain segments at the interface of VL and CL. An increase in the VL–CL angle of 28°

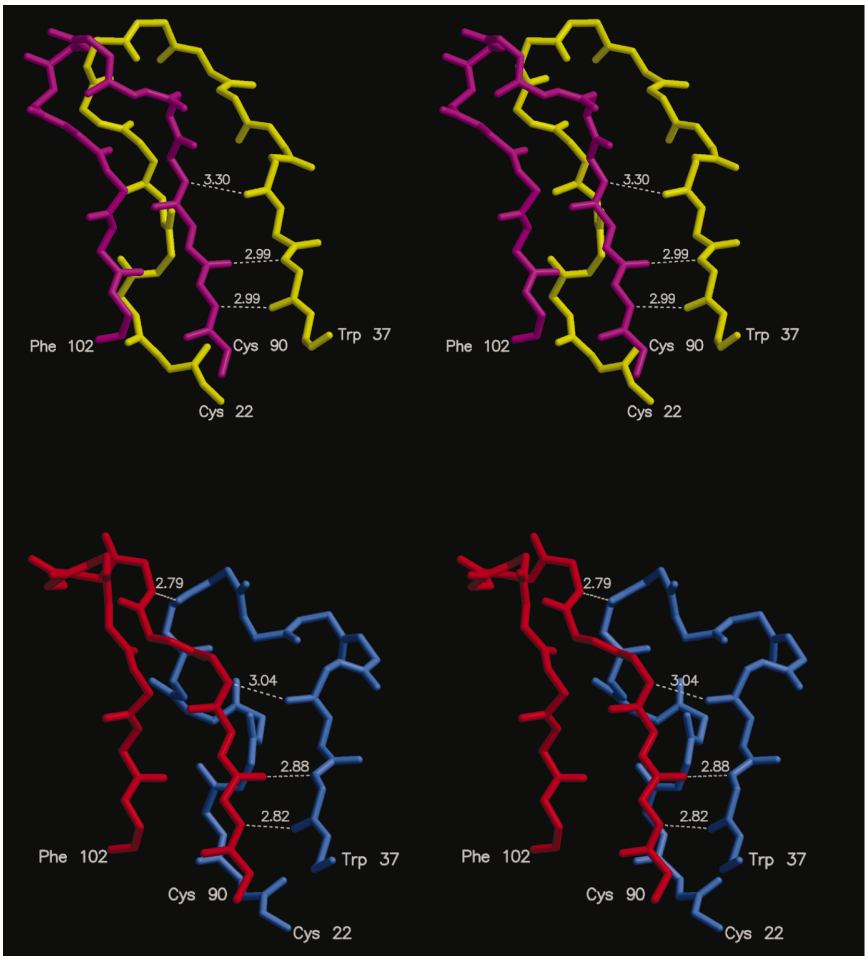

Figure 6
Stereo diagrams of the CDR1 and CDR3 loops in the two conformational isomers of the Sea dimer. CDR1 is yellow in monomer *A* (L-type isomer) and blue in monomer *B* (H-chain analog). CDR3 is magenta in monomer *A* and red in monomer *B*. Hydrogen bonds between CDR1 and CDR3 are designated by dotted lines and the interatomic distances in Å between backbone carbonyl and amide groups are superimposed. Short stretches of antiparallel β-strand pairing occur between the descending arm of the CDR1 loop and the ascending arm of CDR3 in both monomers. Otherwise, the conformations of the CDR1 and CDR3 loops are substantially different in the two isomers. The models were drawn with the program *MOLSCRIPT* (Kraulis, 1991).

in monomer *B* of the Sea dimer allowed components of the four-stranded layer to assume more relaxed conformations similar to those in monomer *A* [the first segment (4-1) of the four-stranded layer is directly connected to the VL domain]. In both Sea monomers, segment 4-1 is divided into two β-strands by a β-bulge consisting of 3–4 residues. Three-stranded layers in both *A* and *B* CL domains are also extremely regular in the Sea dimer (see Fig. 3).

3.7. Malleable regions which may predispose VL domains to become amyloidogenic

While the 'twisted β-pleated sheet conformation' attributed to amyloid fibrils (Glenner, 1980) is built into the structures of all L-chains, the subjects with amyloidogenic properties are generally believed to have regions of instability which predispose them to AL fibrillogenesis (Alim *et al.*, 1999; Pokkuluri *et al.*, 1999). Among human λ-chains, some subgroups are particularly susceptible to AL formation. For example, myeloma-derived λ-chains of subgroup I were found to have a high propensity for producing amyloid-like fibrils *in vitro* after hydrolysis with pepsin (Linke *et al.*, 1973). In comparative studies (Alim *et al.*, 1999), 'Vlambda II' molecules were proposed to have conserved Ser, Thr and Val residues in positions equivalent to 27, 65 and 93 in Fig. 2. Many examples of molecules from subgroup I and II, including Sea and Mcg, have Ser27 in their CDR1 sequences. This is the key residue at the point of impact in the collision of monomer *A* of the Sea protein with a symmetry-related molecule. In Mcg, the part of CDR1 beginning with Ser27 is almost completely disordered in monomer 1, while the same sequence in monomer 2 adopts a well defined helical conformation (Edmundson *et al.*, 1975). These regions are particularly vulnerable because they constitute major crossover segments between the two β-pleated sheets of the VL domain structure. They tend to act as solvent-accessible and expandable (or contractable) springs that respond to local or global movements of the β-pleated sheets.

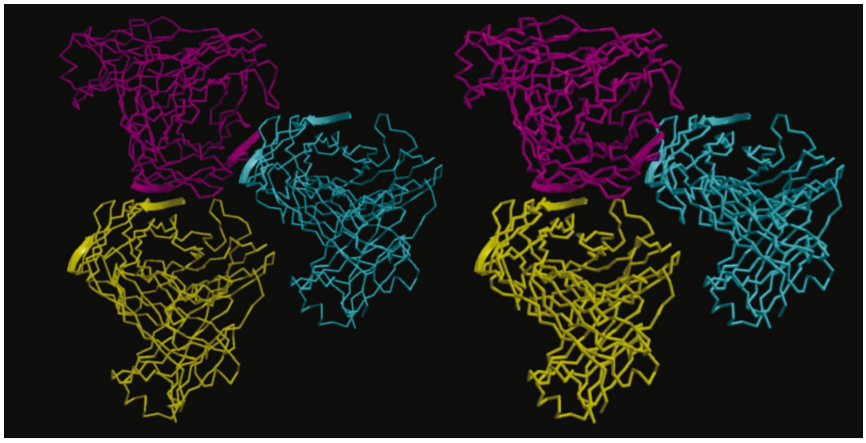

(*a*)

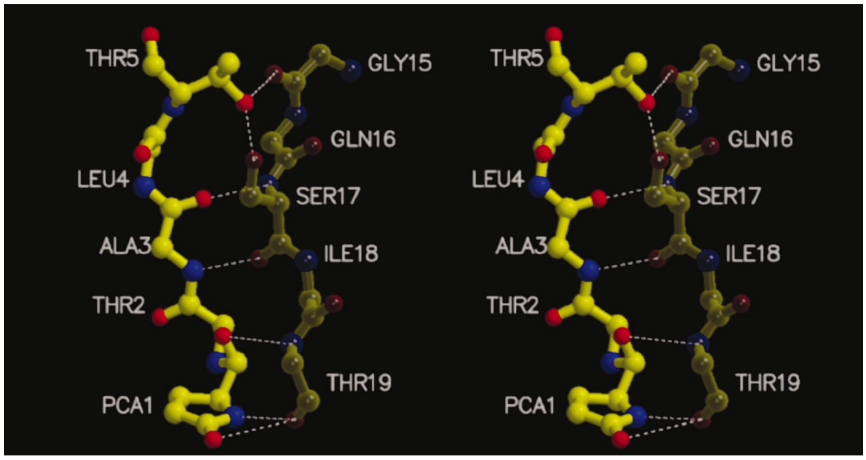

(*b*)

Figure 7
(*a*) Stereo diagram of major packing interactions in the Sea crystal lattice. Two symmetry-related molecules of the Sea dimer are colored magenta (reference molecule) and yellow. A copy of the yellow molecule translated by one unit-cell dimension is colored blue. Arrows designate the β-strands that are paired to form the principal interactions in the nucleation and growth of the crystal. On the left, the magenta arrow designates the β-strand which contains Thr17 and Ser19 of monomer *A*. This strand makes a cross-molecule antiparallel β-pleated sheet with residues 1–5 of monomer *A* in the yellow dimer. On the right, the magenta arrow covers residues 1–5 (monomer *A*) which forms an antiparallel sheet with the β-strand, which includes residues 17–19 in the blue dimer. Such bilateral β-strand pairing interactions continue until they collectively produce a ribbon of molecules of indefinite length in the crystal lattice. (*b*) Stereo representation of the hydrogen bonding in the intermolecular antiparallel β-sheet described above. This figure was produced with the program *MOLSCRIPT* (Kraulis, 1991)

Members of the Vlambda VI subgroup also display an accentuated tendency for amyloid formation. Their sequences have insertions of two residues between residues 68 and 69, which extend a loop adjacent to CDR1. In a crystallographic comparison of two molecules of this subgroup (Pokkuluri *et al.*, 1999), one (Wil) was susceptible to amyloidosis and the other (Jto) participated in ionic and hydrophobic interactions that promoted stability and thereby interfered with fibrillogenesis.

Conveniently for the present discussion, an X-ray analysis in our laboratory is nearing completion for the Mcg × Hud heterodimer. By itself, the Hud λ-chain dimer was obtained from a patient with documented multiple myeloma but no evident fibrillar deposits (Alan Solomon, personal communication). Preliminary examinations of electron-density maps of the Mcg × Hud hybrid indicate no CDR1 instability of the types seen in the Sea and Mcg dimers. An explanation for these observations is now obvious. In the Hud L-chain, proline is substituted for serine in position 27 of the Sea and Mcg proteins and thus renders CR1 much more rigid. Pro15 is retained as in the 'battering-ram' turn of the

Sea protein. Alanine is substituted for Ser14 in Sea, with little consequence in the three-dimensional structure. Mcg has a Ser-Leu sequence in positions 14 and 15.

This work was supported by Grant CA 72803 (to ABE) from The National Cancer Institute, Department of Health and Human Services. We gratefully acknowledge the contributions of The Howard Hughes Medical Institute (to CRM and CAS) and The Maralee and Vernon Jones Foundation (to ABE). For support of our current research, we thank The Oklahoma Center for the Advancement of Science and Technology (OCAST), which has provided Health Research Grant HR 00-093 (to PAR and ABE) and OARS Grant AR 01.2-017 (to ABE).

References

Abola, E. E., Ely, K. R. & Edmundson, A. B. (1980). *Biochemistry*, **19**, 432–439.
Alim, M. A., Yamaki, S., Hossain, M. S., Takeda, K., Yamada, T., Takashi, I. & Shinoda, T. (1999). *Clin. Immunol.* **90**, 399–403.
Alvarado, U. R., DeWitt, C. R., Shultz, B. B., Ramsland, P. A. & Edmundson, A. B. (2001). *J. Cryst. Growth*, **223**, 407–414.
Berman, H. M., Westbrook, J., Feng, Z., Gilliland, G., Bhat, T. N., Weissig, H., Shindyalov, I. N. & Bourne, P. E. (2000). *Nucleic Acids Res.* **28**, 235–242.
Bertram, J., Gualtieri, R. J. & Osserman, E. F. (1980). *Amyloid and Amyloidosis*, edited by G. G. Glenner, P. Pinho e Costa & A. Falcão de Freitas, pp. 351–360. Amsterdam: Excerpta Medica.
Brünger, A. (1992). *Nature (London)*, **355**, 472–475.
Brünger, A. T., Adams, P. D., Clore, G. M., DeLano, W. L., Gros, P., Grosse-Kunstleve, R. W., Jiang, J. S., Kuszewski, J., Nilges, M., Pannu, N. S., Read, R. J., Rice, L. M., Simonson, T. & Warren, G. L. (1998). *Acta Cryst.* D**54**, 905–921.
Buxbaum, J. N., Chuba, J. V., Hellman, G. C., Solomon, A. & Gallo, G. R. (1990). *Ann. Internal Med.* **112**, 455–464.
Crowther, R. A. (1972). *The Molecular Replacement Method: A Collection of Papers on the Use of Non-Crystallographic Symmetry*, edited by M. G. Rossmann, pp. 173–178. New York: Gordon & Breach.
Crowther, R. A. & Blow, D. M. (1967). *Acta Cryst.* **23**, 544–548.
Edmundson, A. B., DeWitt, C. R., Goldsteen, B. & Ramsland, P. A. (1999). *J. Cryst. Growth*, **196**, 276–284.
Edmundson, A. B. & Ely, K. R. (1985). *Mol. Immunol.* **22**, 463–475.
Edmundson, A. B., Ely, K. R., Abola, E. E., Schiffer, M. & Panagiotopoulos, N. (1975). *Biochemistry*, **14**, 3953–3961.
Edmundson, A. B., Ely, K. R. & Herron, J. N. (1984). *Mol. Immunol.* **21**, 561–576.
Edmundson, A. B., Ely, K. R., Herron, J. N. & Cheson, B. D. (1987). *Mol. Immunol.* **24**, 915–935.
Edmundson, A. B., Goldsteen, B. Z., DeWitt, C. R., Fan, Z. C., Shan, L., Faber, C., Hanson, B. L. & Borrebaeck, C. A. K. (1998). *The Immunologist*, **6**, 54–67.
Edmundson, A. B., Harris, D. L., Fan, Z.-C., Guddat, L. W., Schley, B. T., Hanson, B. L., Tribbick, G. & Geysen, H. M. (1993). *Proteins Struct. Funct. Genet.* **16**, 246–267.
Ely, K. R., Herron, J. N., Harker, M. & Edmundson, A. B. (1989). *J. Mol. Biol.* **210**, 601–615.
Esnouf, R. M. (1997). *J. Mol. Graph.* **15**, 132–134.
Falk, R. H., Comenzo, R. L. & Skinner, M. (1997). *N. Engl. J. Med.* **337**, 898–909.
Fitzgerald, P. M. D. (1988). *J. Appl. Cryst.* **21**, 273–278.
Glenner, G. G. (1980). *N. Engl. J. Med.* **302**, 1283–1292.
Glenner, G. G., Ein, D., Eanes, E. D., Bladen, H. A., Terry, W. & Page, D. L. (1971). *Science*, **174**, 712–714.
Harris, D. L., King, E., Ramsland, P. A. & Edmundson, A. B. (2000). *J. Mol. Recogn.* **13**, 198–212.
Herron, J. N., Ely, K. R. & Edmundson, A. B. (1985). *Biochemistry*, **24**, 3453–3459.
Kabat, E. A. & Wu, T. T. (1991). *J. Immunol.* **147**, 1709–1719.
Kabat, E. A., Wu, T. T., Perry, H. M., Gottesman, K. S. & Foeller, C. (1991). *Sequences of Proteins of Immunological Interest.* Bethesda, MD, USA: Public Health Service, US Department of Health and Human Services, National Institutes of Health.
Kraulis, P. J. (1991). *J. Appl. Cryst.* **24**, 946–950.
Kyle, R. A. & Gertz, M. A. (1995). *Semin. Hematol.* **32**, 45–59.
Kyle, R. A., Gertz, M. A., Greipp, P. R., Witzig, T. E., Lust, J. A., Lacy, M. Q. & Therneau, T. M. (1997). *N. Engl. J. Med.* **336**, 1202–1207.
Laskowski, R. A., MacArthur, M. W., Moss, D. S. & Thornton, J. M. (1993). *J. Appl. Cryst.* **26**, 283–291.
Linke, R. P., Zucker-Franklin, D. & Franklin, E. C. (1973). *J. Immunol.* **111**, 10–23.
Matthews, B. W. (1968). *J. Mol. Biol.* **33**, 491–497.
Murshudov, G. N., Vagin, A. A., Lebedev, A., Wilson, K. S. & Dodson, E. J. (1999). *Acta Cryst.* D**55**, 247–255.
Nicholls, A., Sharp, K. A. & Honig, B. (1991). *Proteins*, **11**, 281–296.
Osserman, E. F., Takatsuki, K. & Talal, N. (1964). *Semin. Hematol.* **1**, 3–85.
Otwinowski, Z. & Minor, W. (1997). *Methods Enzymol.* **276**, 307–326.
Pascali, E. (1995). *Crit. Rev. Oncol. Hematol.* **19**, 149–181.
Peabody, D. S., Ely, K. R. & Edmundson, A. B. (1980). *Biochemistry*, **19**, 2827–2834.
Pokkuluri, P. R., Solomon, A., Weiss, D. T., Stevens, F. J. & Schiffer, M. (1999). *Amyloid*, **6**, 165–171.
Rossmann, M. G. (1990). *Acta Cryst.* A**46**, 73–82.
Shaw, D. C., Harris, D. L., He, X. M., Oster, J. A., Montgomery, D. L., Ely, K. R. & Edmundson, A. B. (1987). *Mol. Immunol.* **24**, 267–274.
Solomon, A. & Weiss, D. T. (1995). *Amyloid Int. J. Exp. Clin. Invest.* **2**, 269–279.
Stevenson, G. T. & Straus, D. (1968). *Biochem. J.* **108**, 375–382.
Stone, M. J. (1990). *Blood*, **75**, 531–545.
Sunde, M. & Blake, C. (1997). *Adv. Protein Chem.* **50**, 123–59.
Wall, J., Murphy, C. L. & Solomon, A. (1999). *Methods Enzymol.* **309**, 204–217.
Wünsch, E. K. & Heidrich, J. G. (1963). *Hoppe-Seyler's Z. Physiol. Chem.* **333**, 149–162.